Frontiers in Bioscience Landmark

Front. Biosci. (Landmark Ed) **2026**; 31(2): 46641
https://doi.org/10.31083/FBL46641

Original Research

Ferroptosis Induction is Insufficient to Ensure NK Cell Activation in High-Grade Ovarian Cancer

Cinzia Garofalo[1,*,†], Stefania Scicchitano[1,†], Eleonora Vecchio[1,*], Antonia Nisticò[2], Barbara Quaresima[1], Beatrice Stella[1], Carmela De Marco[3], Flavia Biamonte[1], Maria Concetta Faniello[1]

[1]Research Center of Biochemistry and Advanced Molecular Biology, Department of Experimental and Clinical Medicine, "Magna Graecia" University of Catanzaro, 88100 Catanzaro, Italy
[2]SOC di Immunoematologia e Medicina Trasfusionale, Azienda Ospedaliero Universitaria "Renato Dulbecco", 88100 Catanzaro, Italy
[3]Department of Experimental and Clinical Medicine, University "Magna Graecia" of Catanzaro, Campus "S. Venuta", 88100 Catanzaro, Italy
*Correspondence: cinziagarofalo@unicz.it (Cinzia Garofalo); eleonoravecchio@unicz.it (Eleonora Vecchio)
[†]These authors contributed equally.
Academic Editor: Sung Eun Kim
Submitted: 16 September 2025 Revised: 3 December 2025 Accepted: 9 December 2025 Published: 5 February 2026

Abstract

Background: High-grade ovarian cancer (HGOC) is a heterogeneous and aggressive malignancy with a tumor microenvironment (TME) that suppresses immune responses, limiting immunotherapy efficacy. Ferroptosis, an iron-dependent form of regulated cell death, has emerged as a potential therapeutic target. **Methods**: We investigated the immunomodulatory effects of the ferroptosis inducer RAS-Selective Lethal 3 (RSL3) in four HGOC cell lines (ES-2, OVCAR-5, HEY, PEO-1) using flow cytometry and lactate dehydrogenase (LDH) release assays. **Results**: RSL3 modulated Natural Killer (NK) ligand expression in a cell line-dependent manner, resulting in differential susceptibility to NK cell-mediated cytotoxicity. OVCAR-5 cells became more susceptible to NK cell killing after treatment, whereas HEY cells showed reduced susceptibility, and ES-2 and PEO-1 cells exhibited minimal changes. **Conclusions**: Ferroptosis induction alone does not consistently enhance NK cell-mediated cytotoxicity in HGOC cells. These findings underscore the heterogeneity of tumor responses and highlight the need for further studies, particularly in *in vivo* models, to elucidate mechanisms linking ferroptosis to immune recognition and thereby inform therapeutic development.

Keywords: high-grade ovarian cancer; tumor microenvironment; NK cells; ferroptosis; RSL3

1. Introduction

Among gynecologic malignancies, human ovarian cancer shows one of the highest mortality rates, contributing to over 200,000 deaths worldwide annually [1]. Ovarian carcinomas are classified into three different subtypes: epithelial (Epithelial Ovarian Cancer (EOC), the most widespread), germ cell and sex-cord-stromal types. The epithelial type is further subdivided into high-grade and low-grade serous, endometrioid, clear cell, and mucinous sub-types [2]. High-grade serous ovarian cancer (HGSOC) accounts for most epithelial ovarian carcinomas (around 70%), whereas Clear Cell Ovarian Cancer (CCOC) represents approximately 5–10% of cases. Both sub-types are characterized by chemoresistance and poor prognosis [3,4]. Despite the therapeutic potential of immunotherapy in promoting effective immune surveillance, long-term clinical benefit has been observed in only about 10–15% of ovarian cancer patients, according to phase III clinical evidence [5–10]. The limited efficacy of immunotherapy is mostly attributed to the immunosuppressive tumor microenvironment (TME), which impairs effective immune surveillance and cytotoxic innate and adaptive immune responses [11–15].

Natural Killer (NK) cells, a type of group 1 of innate lymphoid cells (ILCs), play a fundamental role in early defense against stressed, virally infected and transformed cells [16,17]. Unlike $CD8^+$T cells, NK cells directly induce target cell death without any prior sensitization. NK cells are further distinguished into two major sub-populations, based on the absence of CD3 (T cell lineage marker) and the expression of CD56 (NK cell lineage marker): $CD56^{bright}$ and $CD56^{dim}$, representing 10% and 90% of all peripheral blood NK cells respectively. $CD56^{bright}$ NK cells exhibit a low cytotoxic potential and are mainly immunoregulatory, while $CD56^{dim}$ NK cells display strong cytotoxicity but limited secretory capabilities [18,19]. NK cells activity is tightly regulated by the balance between activating and inhibitory signals, mediated by receptor ligand interactions. Lack of inhibitory molecules on tumors or virus-infected cells is insufficient to activate NK cells, signaling from activating molecules is also necessary [16,20]. This intriguing mechanism is based on the "Missing-self hypothesis" [21]. Although infiltrating NK cells in ovarian cancer is associated with improved patient prognosis [22–24], recent studies indicate that the immunosuppressive TME compromises NK cell function [25–27].

Among the emerging modulators of immune response is ferroptosis, a non-apoptotic, iron-dependent type of regulated cell death (RCD) characterized by the accumulation of lipid peroxides and reactive oxygen species (ROS) [28,29]. Notably, ovarian cancer exhibits resistance to ferroptosis, a condition that may support the use of ferroptotic inducers (FINs) alone or in combination with traditional therapies to enhance treatment efficacy [30]. Several studies demonstrate that FINs, when combined with docetaxel, enhance chemosensitivity in preclinical models of ovarian cancer [31,32]. Moreover, the combination of FINs with cisplatin-based chemotherapy increases drug cytotoxicity and reduces adverse effects *in vitro* and *in vivo* models [33]. In preclinical ovarian cancer models, immunotherapy synergizes FINs, highlighting their potential as pharmacological candidates for combination therapies [34,35]. Lang and colleagues [36] demonstrated that ferroptosis induced by chemotherapy, radiotherapy, or immunotherapy enhances dendritic cell recruitment, promotes antigen presentation, and activates cytotoxic lymphocytes, *in vivo* and *in vitro* models [36].

Although ferroptosis has been shown to influence adaptive immune responses [36], its effects on innate immune cells, particularly in the context of ovarian cancer, remain poorly understood. In particular, the impact of ferroptotic cell death on NK cell recognition against high-grade ovarian cancer (HGOC) has not been investigated to date.

In this study, we induced ferroptosis in HGOC cells using RAS-Selective Lethal 3 (RSL3), a Glutathione Peroxidase 4 (GPX4) inhibitor, to evaluate its impact on NK cell activation and cytotoxicity. Our results show that ferroptosis modulates the expression of several immune ligands on the tumor cell surface, including Poliovirus Receptor (PVR), Programmed Death-Ligand 1 (PD-L1), Unique Long 16-Binding Protein 2 (ULBP2), MHC class I chain-related protein (MIC) A and B (MICA/B), and Nectin-like molecules-2 (Nectin-2). However, NK cells do not consistently recognize or respond to ferroptotic cancer cells, suggesting that RSL3 alone may be insufficient to trigger a robust NK cell–mediated immune response. These findings provide new insights into the interplay between ferroptosis and innate immunity in ovarian cancer.

2. Materials and Methods

2.1 Cell Lines and Culture Conditions

Human epithelial ovarian cancer (hEOC) cell lines, ES-2 (High grade ovarian clear cell adenocarcinoma), OVCAR-5 (High grade ovarian serous adenocarcinoma), HEY (High grade ovarian serous adenocarcinoma) and PEO-1 (High grade ovarian cystadenocarcinoma) were purchased from the American Type Culture Collection (ATCC, Manassas, VA, USA). ES-2 and PEO-1 cells were cultured in RPMI 1640, whereas OVCAR-5 and HEY cells were maintained in DMEM medium. All media were supplemented with 10% foetal bovine serum, 50 U/mL of penicillin, and 50 µg/mL of streptomycin (Thermo Fisher Scientific, Milan, Italy). Cells were cultured at 37 °C in a humidified incubator with 5% CO_2 atmosphere. ES-2 and HEY cells were plated at a concentration of 2.0 $\times$ 10^5 cells/well in a 6 well plate, while OVCAR-5 and PEO-1 cells were plated at a concentration of 2.5 $\times$ 10^5 cells/well. After 24 hours, the medium was removed, cells were washed with PBS1X, and RSL3 ((1S,3R)-RSL3), Cat. HY-100218A/CS-5650, MedChemExpress, D.B.A., Milan, Italy) or RSL3 and Ferrostatine-1 (Fer-1) (Ferrostatine-1, AMBH303C51A, Merk Life Science S.r.l., Milan, Italy) conditioned medium was added for 24 hours. Untreated cells were used as control. All experiments were performed between the first (p1) and the 4th (p4) passage of cell culture. All cell lines were validated by STR profiling and tested negative for mycoplasma (MycoAway™ 1000X Mycoplasma Cocktail, G398 ABM; Mycoplasma PCR Detection Kit G238, Applied Biological Materials Inc., Viking Way Richmond, Canada).

2.2 Cell Viability Assays

To assess RSL3 toxicity, ES-2, HEY, OVCAR-5 and PEO-1 cells were treated with the following concentrations of RSL3: (ES-2: 50 nM, 100 nM, 200 nM; HEY: 1 µM, 2 µM, 6 µM; OVCAR-5: 2.5 µM, 5 µM, 10 µM; PEO-1: 5 µM, 10 µM, 15 µM). To assess Fer-1 toxicity, PEO-1 cells were treated at different concentrations of Fer-1 (5 µM, 10 µM, 15 µM) and ES-2, HEY and OVCAR-5 cells were treated respectively with 1, 10 and 2 µM of Fer-1concentration as indicated in [37–39]. Co-treatment with RSL3 and Fer-1 was performed for each cell line. Cells were processed as already described [40]. Briefly, 1 $\times$ 10^5 cells with different treatments were collected and were incubated with propidium iodide (PI) at 37 °C for 15 min in the dark. After the incubation, 400 µL of PBS (1$\times$) was added, and all samples were acquired by FACS BD LSRFortessa™ X-20 cytofluorimeter (BD Biosciences, San Jose, CA, USA), measuring PI (PE) fluorescence against the forward scatter parameter (FSC-A). Data were analysed by FlowJo™ v10 Software (BD Biosciences, San Jose, CA, USA). Untreated cells were used as a control.

The growth rates of cells were obtained using the Trypan Blue dye exclusion method. Cell viability of ES-2, HEY, OVCAR-5, and PEO-1 was also evaluated with the CellTiter-Glo® Luminescent Cell Viability Assay (Promega, Madison, WI, USA), which is based on the quantitation of ATP as an indicator of metabolically active cells as previously described [41,42]. Briefly, cells were plated in 96 wells overnight and the next day, were treated or not with different concentrations of RSL3 for 24 h. Each experiment was performed in technical and biological triplicates. Half-maximal inhibitory concentrations (IC_{50}) were calculated by plotting a dose-response curve using non-linear regression analysis using GraphPad Prism V9 software (GraphPad Software, Boston, MA, USA).

2.3 Apoptosis Assay

Apoptosis assay was assessed as already described [43]. Briefly, a number of 1×10^5 of untreated and RSL3, Fer-1 or RSL3 and Fer-1 treated cells (ES-2, HEY, OVCAR-5 and PEO-1), were double-stained with Annexin V and PI (Alexa Fluor®488 Annexin V/Dead Cell Apoptosis Kit, Thermo Fisher Scientific) for 15 min at RT in the dark. 400 µL of Binding Buffer was added, and all samples were acquired by FACS BD LSRFortessaTM X-20 cytofluorometer (BD Biosciences), measuring PI (PE) fluorescence against Annessin V (FITC) fluorescence. Data were analysed by FlowJo™ v10 Software (BD Biosciences). Untreated cells were used as a control. Each experiment was performed in technical and biological triplicates.

2.4 Intracellular ROS Detection

Intracellular ROS production was quantified through the redox sensitive probe 2′-7′-Dichlorodihydrofluorescein diacetate (CMH2DCFDA) (Thermo Fisher Scientific). ES-2, HEY, OVCAR-5 and PEO-1 were treated with RSL3, Fer-1 or RSL3 and Fer-1 Cells were incubated with CMH2DCFDA for 30 min at 37 °C. Thereafter, cells were centrifuged and resuspended in 200 µL of PBS (1×). Samples were acquired by FACS BD LSRFortessaTM X-20 cytofluorometer (BD Biosciences) and data were analysed with FlowJo v10 Software (BD Biosciences). Untreated cells were used as a control. Each experiment was performed in technical and biological triplicates. Gating strategy is indicated in **Supplementary Fig. 1A**.

2.5 Mitochondrial ROS Detection

Mitochondrial ROS production was assessed in both untreated and treated cells (ES-2, HEY, OVCAR-5 and PEO-1) with RSL3, Fer-1 or RSL3 and Fer-1. Single cell suspensions were incubated with MitoSOX (MitoSOX Red Mitochondrial Superoxide Indicator (Thermo Fisher Scientific, Waltham, MA, USA) for 30 min at 37 °C. Thereafter, cells were centrifugated and resuspended in 200 µL of PBS (1×). Samples were acquired by FACS BD LSRFortessaTM X-20 cytofluorometer (BD Biosciences) and data were analysed with FlowJo v10 Software (BD Biosciences). Untreated cells were used as a control. Each experiment was performed in technical and biological triplicates. A gating strategy is indicated in **Supplementary Fig. 1A**.

2.6 Lipid Peroxidation Assay

Lipid peroxidation was investigated as previously described [35]. ES-2, HEY, OVCAR-5 and PEO-1 cells untreated and treated with RSL3, Fer-1 or RSL3 and Fer-1, were incubated with BODIPY (BODIPY™ 581/591C11 dye (Thermo Fisher Scientific) for 30 min at 37 °C. Cells were washed twice with PBS (1×). Oxidation of BODIPY-C11 was observed by a shift of the fluorescence emission peak from ~590 nm to ~510 nm, directly correlated with lipid ROS generation. Samples were acquired by FACS BD LSR Fortessa TM X-20 cytofluorometer (BD Biosciences) and data were analysed with FlowJo v10 Software (BD Biosciences). Untreated cells were used as a control. Each experiment was performed in technical and biological triplicates. A gating strategy is indicated in **Supplementary Fig. 1A**.

2.7 Peripheral Blood Monocytes Cells (PBMCs) Isolation and NK Cells Purification

To obtain NK cells, we first separated PBMCs from buffy coats provided by healthy donors using a standard density gradient centrifugation protocol [44]. Buffy-coats from healthy volunteers were supplied by the blood transfusion center of Pugliese-Ciaccio Hospital, Catanzaro, Italy, previous consent to the processing of personal data. In accordance with Italian regulations (Legislative Decree 196/2003 as amended by Legislative Decree 101/2018, and EU Regulation 2016/679 – GDPR), this study used residual biological material collected for routine diagnostic purposes. All samples were anonymized prior to analysis. No additional procedures or interventions were performed for research purposes. In line with national regulations, this type of retrospective, anonymized analysis does not require approval from an ethics committee. All procedures were conducted in compliance with the Declaration of Helsinki and institutional guidelines. Blood samples were divided into Falcon tubes according to the protocol described in [44]. For each tube, an equal volume (1:1) of PBS (1×) and Lymphocyte Separation Medium (density 1.007 g/mL; Sigma Aldrich, Merck KGaA, Darmstadt, Germania) was added. The samples were then centrifuged at 2200 rpm for 30 minutes without brake. After the centrifugation, white ring cells were collected, washed twice with PBS (1×) and were incubated with a red blood cell lysis buffer (Sigma Aldrich, Merck, Germany) at RT for 15 min. After the incubation, cells were washed with PBS1X and were cultured overnight at a concentration of 1.0×10^6 cells/mL. The day after, cells were centrifuged and NK cells were isolated by using human NK Cell Isolation Kit (Miltenyi Biotec, Bergisch Gladbach, Germany). Cells were counted and incubated with NK Cell Biotin-Antibody Cocktail (for 5 min at 2–8 °C) and subsequently they were incubated with NK Cell MicroBead Cocktail (for 10 min at 2–8 °C). After the incubation, we proceed to subsequent magnetic cell separation. NK Isolation kit ensures around 95% of purity. To verify this, once isolated, purified NK cells were stained with CD56 and CD3 and analyzed by flow cytometry. PBMCs were used as control. Cell debris and dead cells were excluded by using viability marker (BD Horizon™ Fixable Viability Stain 780) (SSC vs viability fluorescence). Purified resting NK cells were used for cytotoxicity assay. The gating strategy is indicated in **Supplementary Fig. 1C**.

2.8 Immune Phenotype Analysis

After the incubation with RSL3, ES-2, HEY, OVCAR-5 and PEO-1 cells were collected and incubated with a viability marker (BD Horizon™ Fixable Viability Stain 780) for 15 min at RT in the dark. A number of 2 × 10^5 cells were used for each tube. Then, cells were washed twice with PBS (1×) and were marked with the following antibodies: APC anti-human CD274 (B7-H1, PD-L1; clone 29E.2A3)/IgG2b, PE anti-human MICA/MICB (clone 6D4)/IgG2a, APC anti human CD155 (PVR) (clone SKII.4)/IgG1, PE anti-human CD112 (Nectin-2) (clone TX31)/IgG1 were purchased from BioLegend (San Diego, CA, USA); PE anti-human ULBP-2/5/6 (clone FAB1298P)/IgG2a were purchased from R&D Systems (Minneapolis, MN, USA). Cells were maintained for 30 minutes at +4 °C in the dark and subsequently centrifugated and pellets were resuspended with 200 µL of FACS FLOW and were acquired by FACS BD LSRFortessaTM X-20 cytofluorometer (BD Biosciences).

Voltages for physical parameters (SSC, FSC) and fluorescence channels were previously optimized for each cell line used. After identifying the population of interest, live cells were discriminated against from dead cells using an SSC-A vs viability marker plot. Subsequently, all markers were acquired on the live cell population gate (viability marker-negative). Data was analyzed with FlowJo v10 Software (BD Biosciences). Untreated cells were used as a control. Each experiment was performed in technical and biological triplicates. The gating strategy is indicated in **Supplementary Fig. 1B**.

2.9 Cytotoxicity Assay

Cytotoxicity assay was performed as already described [45]. After 24 hours of incubation with RSL3, target cells were detached with trypsin, centrifuged at 1500 rpm for 5 min and counted with trypan blue. Target cells were subsequently plated with purified NK cells in nude RPMI-1640 medium in 96 well U-bottom plates. The experiments were performed starting from 50:1 (500.000:10.000) Effector to Target Ratio(E:T). Co-cultures were incubated in a humidified 5% CO_2 incubator at 37 °C for three hours. After centrifugation at 250 ×g for 10 min the supernatants were collected and transferred into a96 well, flat-bottom micro-plate. Cells were incubated with freshly prepared reaction mixture (Cytotoxicity Detection Kit lactate dehydrogenase (LDH) (Roche) for 30 min at 37 °C. LDH activity was determined with the multiwell reader (Multiskan Microplate Spectrophotometer, Thermo Fisher Scientific, Waltham, MA, USA), with a sample's absorbance at 490 nm. The percentage of target cell lysis was calculated as follows: cytotoxicity (%) = (target cell mix – low control) / (high control – low control) × 100. Untreated cells were used as a control. All the experiments were performed in technical and biological triplicates.

2.10 Expression Analysis by qRT- PCR

A total of 1 µg of RNA, previously prepared using PureLink RNAMini Kit (Thermo Fisher Scientific) and verified using a NanoDrop 2000/2000c Spectrophotometer (Thermo Fisher Scientific), was used to synthesize cDNA using SuperScript III reverse transcriptase and was amplified with the iQ™ SYBR® green super mix (Bio-Rad, Milan, Italy) using the qRT-PCR amplifier QuantStudio3 (Applied Biosystems, Milan, Italy) [46]. Reactions were carried out in triplicate, and the analysis of gene expression was calculated as 2^{-ddCt} and normalized for the house-keeping gene (Glyceraldehyde-3-Phosphate Dehydrogenase (GAPDH)). Primers used in this study were as follows (5-3):

h-GPX4 (fwd) ATCGACGGGCACATGGTTAA,
h-GPX4 (rev) CGACGAGCTGAGTGTAGTTT.
h-NRF2 (fwd) CACCACCCACACAACTTACTGC,
h-NRF2 (rev) GGTCTTCTTGGGGCTTAGGT.
h-CD71 (fwd) TGCTGCTTTCCCTTTCCTTG,
h-CD71 (rev) GCTCGTGCCACTTTGTTCAA.
h-GAPDH (fwd) CACCATCTTCCAGGAGCGAG,
h-GAPDH (rev) TCAC-GCCACAGTTTCCCGGA.

2.11 Protein Extraction and Western Blotting

Total extracts were prepared as previously described [47]. Briefly, to obtain total protein extracts, cells were washed once with PBS (1×) and total cell lysates were prepared using RIPA. The samples were centrifuged at 12,000 rpm for 20 min at +4 °C and supernatants containing the total extracts were recovered. Proteins were separated on 4–12% NuPAGENovexBis-Tris protein gradient polyacrylamide gels (Thermo Fisher Scientific) and blotted onto nitrocellulose. Membranes were blocked with 5% milk (BioRad) and then incubated with the following antibodies: GPX4 with a rabbit anti-GPX4 (1:500, ab41787), NRF2 with a mouse anti-NRF2 (1:500, sc-365949, Santa Cruz, Milan, Italy) antibody, CD71 with a rabbit anti-CD71 (1:1000, D7S5Z, Cell Signaling Technology, Milan, Italy) antibody and GAPDH with an anti-GAPDH-HRP conjugated (1:1000, sc-47724). Peroxidase AffiniPure Sheep Anti-Mouse IgG, Peroxidase AffiniPure Donkey Anti-Rabbit IgG, Peroxidase AffiniPure Donkey Anti-Mouse IgG (1:10,000, Jackson ImmunoResearch Europe Ltd. Cambridge House) secondary antibodies were used. Signals were detected using the WESTARï2.0 ECL substrates for Western blotting (XLS070,0250, Cyanagen, Bologna, Italy) and acquired using a Uvitec Alliance Mini HD9 (Uvitec, Cambridge, UK).

2.12 Statistical Analysis

All experiments were performed in triplicate, and data are presented as the mean ± standard deviation (SD). Statistical comparisons were conducted using paired two-tailed Student's *t*-tests in GraphPad Prism 5.0. Statistical significance was denoted as follows: $p < 0.05$ (*), $p < 0.01$ (**), $p < 0.001$ (***) [42].

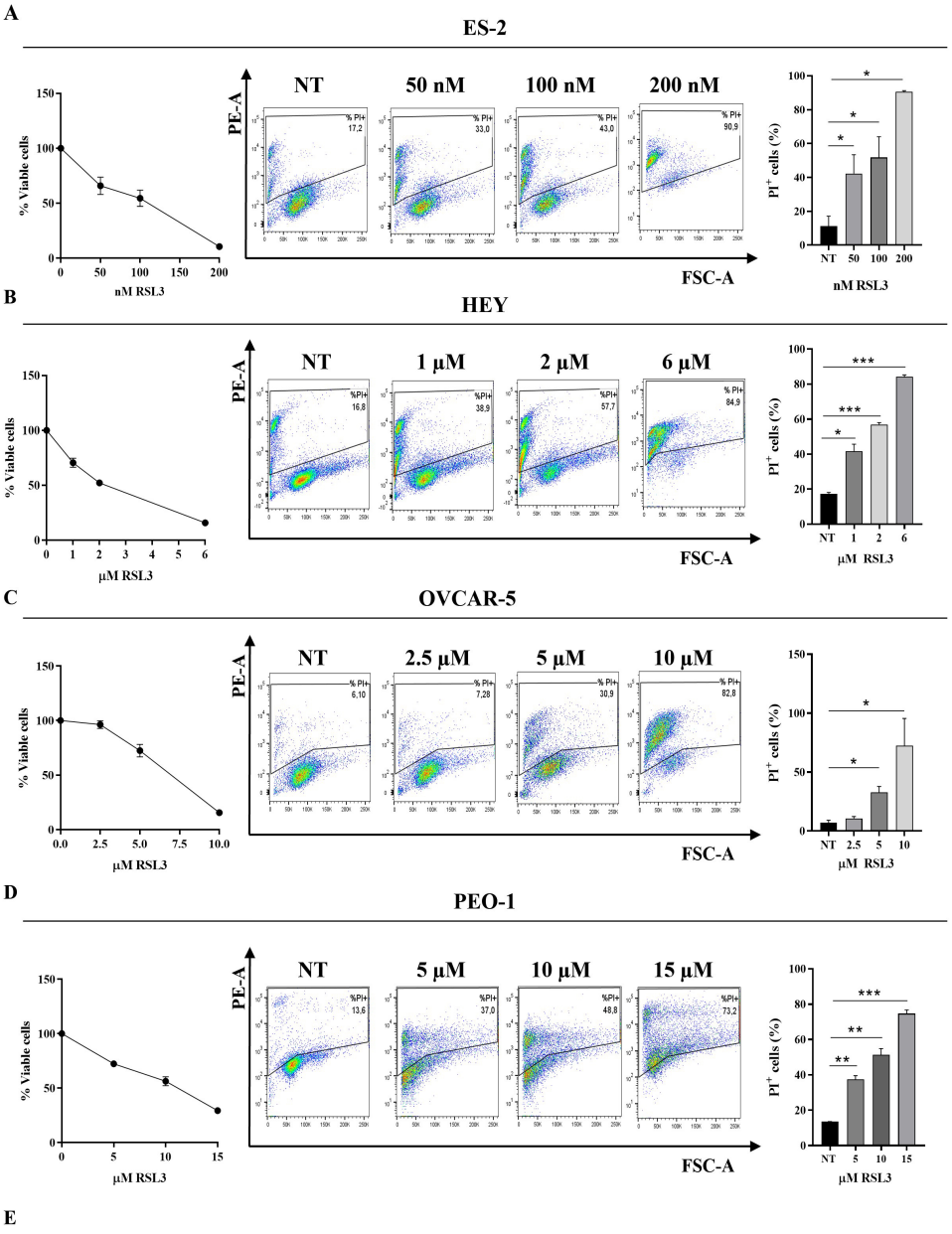

E

RSL3	
Cell line	**IC_{50} values**
OVCAR5	7.22 µM
ES-2	90.04 nM
HEY	1.98 µM
PEO-1	9.96 µM

Fig. 1. Dose-dependent RAS-Selective Lethal 3 (RSL3) cytotoxicity on human ovarian cancer cell lines. Ovarian cancer cell lines were treated with RSL3 for 24 hours at the following concentrations: (A) ES-2: 50, 100, 200 nM; (B) HEY: 1, 2, 6 µM; (C) OVCAR-5: 2.5, 5, 10 µM; (D) PEO-1: 5, 10, 15 µM. The IC_{50} of RSL3 was determined for all cell lines (A–D left panel). The percentage of dead cells (propidium iodide (PI) positive) is reported in each representative plot (A–D, middle panel). Statistical analysis of % of PI positive cells untreated (NT) and treated with RSL3 was reported for each cell line tested (A–D right panel). All the experiments were performed in technical and biological triplicates. Data were represented as means ± SD; ***p-value < 0.001; **p value < 0.01; *p value < 0.05. A paired two-tailed Student's t test was used. (E) RSL3 IC_{50} cell viability on high-grade ovarian cancer (HGOC) was assessed through Cell Titer Glo following treatments with increasing amounts of RSL3 for 24 hours.

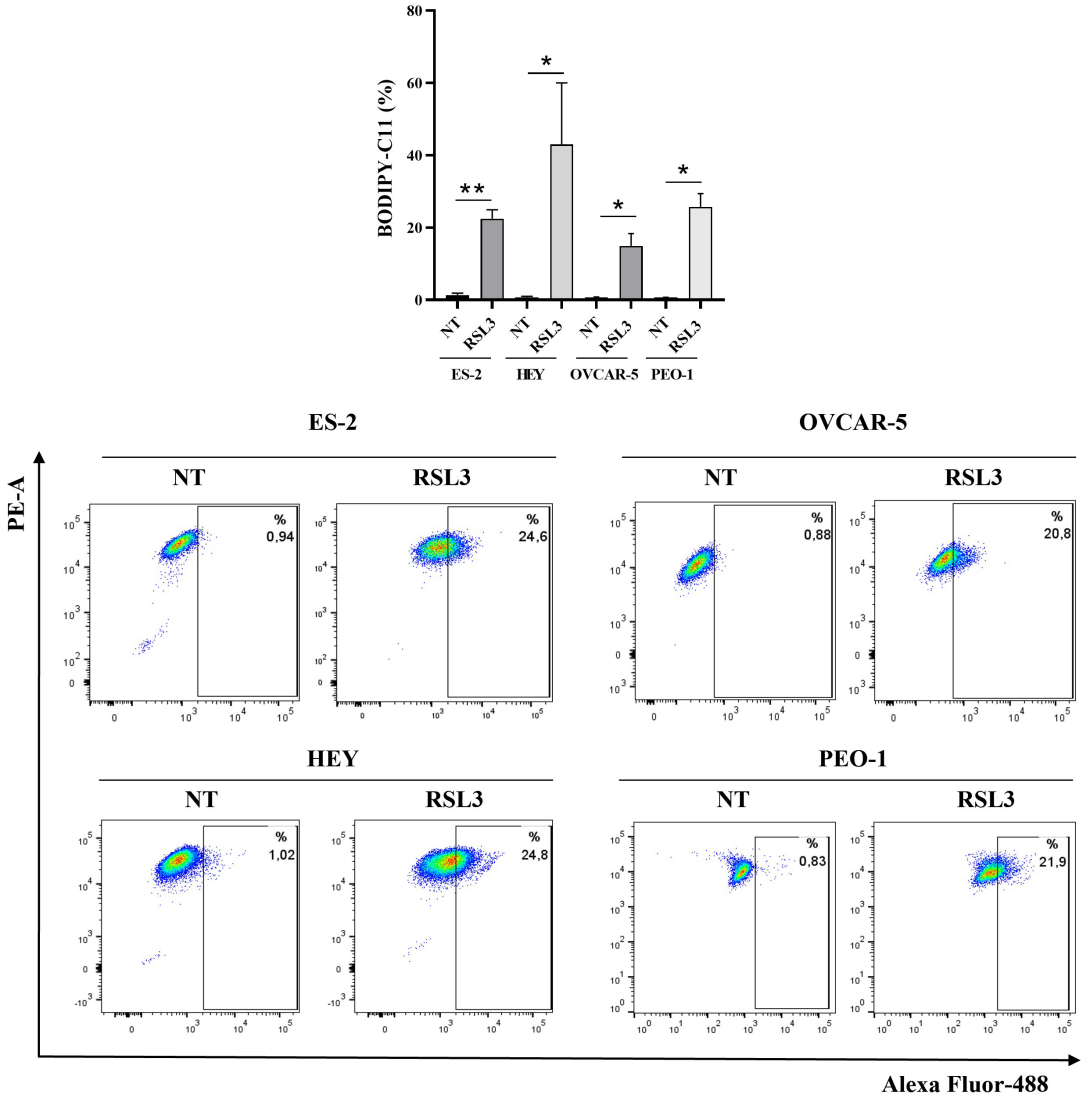

Fig. 2. RSL3 induces lipid peroxidation in ovarian cancer cell lines. Statistical analysis (upper panel) and representative plots (bottom panel) of the percentage of positive cells for BODIPY-C11 are reported. Cells were treated with RSL3 for 24 hours at the following concentrations: 50 nM (ES-2), 1 µM (HEY), 5 µM (OVCAR-5) and 5 µM (PEO-1). All the experiments were performed in technical and biological triplicates. Data were represented as means ± SD. **p-value < 0.01; *p-value < 0.05. A paired two-tailed Student's t test was used.

3. Results

3.1 RSL3 Induces Ferroptosis in HGOC Cells

To assess whether RSL3 modulates NK cell-mediated response against ovarian cancer, the following cell lines (ES-2, HEY, OVCAR-5 and PEO-1) were treated with increasing concentrations of RSL3 for 24 hours (Fig. 1). For the purposes of this study, a concentration of RSL3 slightly below the IC_{50}, resulting in moderate cell death ($\sim$ 40%), were selected (Fig. 1). The IC_{50} value for each cell line is reported on Fig. 1. Flow cytometry analysis confirmed the induction of ferroptosis in RSL3-treated HGOC cell lines (Figs. 2,3). RSL3 treatment significantly increased lipid peroxidation (RSL3 treated vs NT: 16.5× fold, p value 0.003 for ES-2; 3.84× fold, p value 0.04 for HEY; 20.5× fold, p value 0.02 for OVCAR-5; 1.36× fold, p value 0.02 for PEO-1; Fig. 2), mitochondrial ROS (RSL3 treated vs NT: 1.25× fold, p value 0.004 for ES-2; 2× fold, p value 0.04 for HEY; 1.76× fold, p value 0.01 for OVCAR-5; 1.5× fold, p value 0.0003 for PEO-1; Fig. 3A) and total intracellular ROS (RSL3 treated vs NT: 3.47× fold, p value 0.008 for ES-2; 2.65× fold, p value 0.0001 for HEY; 1.72× fold, p value 0.02 for OVCAR-5; 1.79× fold, p value 0.0001 for PEO-1 levels; Fig. 3B). Co-treatment with Ferrostatin-1 (Fer-1), a ferroptosis inhibitor, and RSL3 restored cellular viability (**Supplementary Fig. 2A**) together with intracellular ROS levels and lipid peroxidation

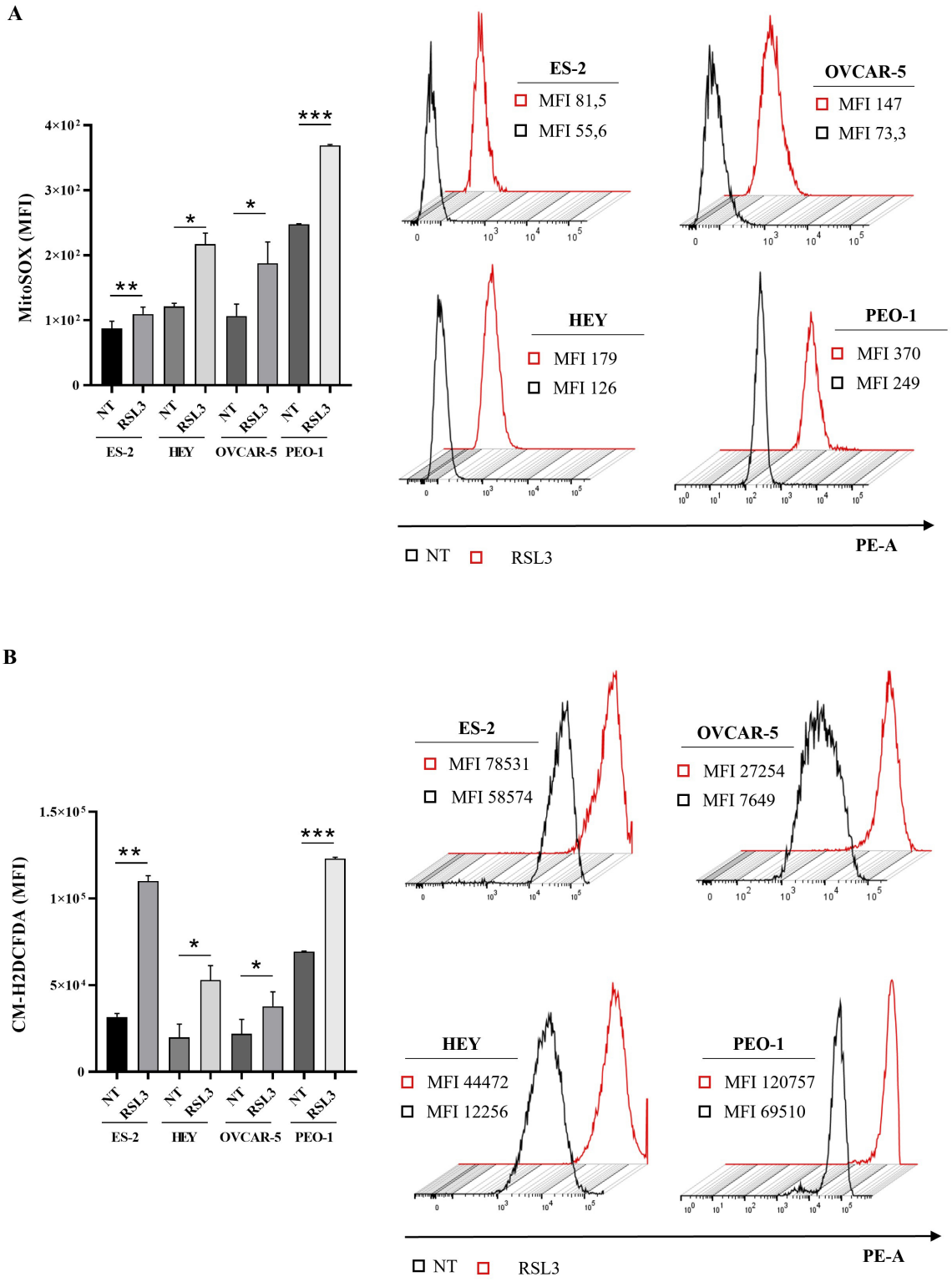

Fig. 3. RSL3 enhances intracellular reactive oxygen species (ROS) in ovarian cancer cell lines. (A) Statistical analysis of Median Fluorescence Intensity (MFI) (left panel) and representative histograms (right panel) of MitoSOX are reported. (B) Statistical analysis of MFI (left panel) and representative histograms (right panel) of CM-H2DCFDA are reported. Cells were treated with RSL3 for 24 hours at the following concentrations: 50 nM (ES-2), 1 μM (HEY), 5 μM (OVCAR-5), 5 μM (PEO-1). All the experiments were performed in technical and biological triplicates. Data were represented as means ± SD. ***p-value < 0.001; **p-value < 0.01; *p-value < 0.05. A paired two-tailed Student's t test was used.

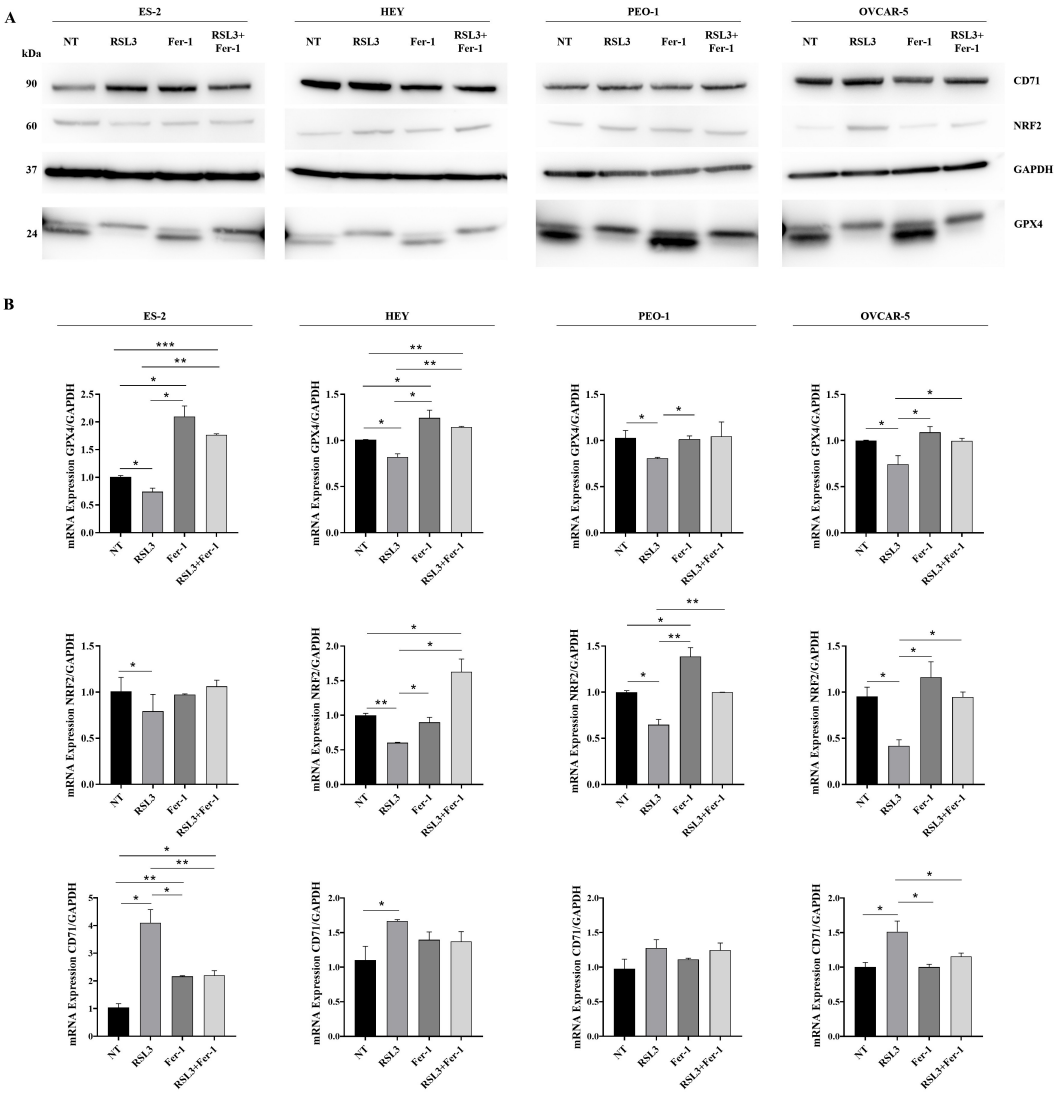

Fig. 4. RSL3 induces mRNA and protein expression of ferroptosis-associated markers in HGOC cell lines. Cells were treated with RSL3 or Fer-1 alone or co-treated with RSL3 and Ferrostatin-1 (Fer-1) for 24 hours (NT indicates untreated cells). Proteins and total RNA, extracted from human ovarian cancer cell lines, were analysed by western blot (A) and qRT-PCR (B) for the expression of GPX4, NRF2 and CD71 in ES-2, HEY, OVCAR-5 and PEO-1. Results were normalized using GAPDH as the housekeeping protein or gene. All experiments were performed in technical and biological triplicates. Asterisks indicate **p*-value < 0.05, ***p*-value < 0.01, ****p*-value < 0.001. A paired two-tailed Student's *t* test was used. GPX4, Glutathione Peroxidase 4; NRF2, Nuclear factor erythroid 2-related factor 2; GAPDH, Glyceraldehyde-3-Phosphate Dehydrogenase.

to those observed in untreated cells (**Supplementary Fig. 2B**), effectively preventing ferroptotic cell death. Western blotting (Fig. 4A and **Supplementary Fig. 3**) and qRT-PCR (Fig. 4B) analyses confirmed RSL3-induced ferroptosis. *CD71* mRNA levels were significantly increased in ES-2, HEY, and OVCAR-5 cells (RSL3 vs NT: *p* value 0.010 for ES-2; *p* value 0.032 for HEY; *p* value 0.025 for OVCAR-5), while a slight, but not significant, change was observed in PEO-1 cells. At the protein levels, CD71 was significantly increased only in ES-2 and PEO-1 cells (RSL3 vs NT: *p* value 0.002 for ES-2; *p* value 0.028 for PEO-1), whereas changes in HEY and OVCAR-5 were not statistically significant. *NRF2* mRNA levels were significantly reduced in all cell lines (RSL3 treated vs NT: *p* value 0.016 for ES-2; *p* value 0.001 for HEY; *p* value 0.013 for PEO-1; *p* value 0.016 for OVCAR-5). At the protein level, NRF2 was significantly decreased only in ES-2 cells (RSL3 vs NT: *p* value 0.014), while increased levels were observed in HEY and OVCAR-5 cells (RSL3 vs NT: *p* value 0.0001 for HEY; *p* value 0.0004 for OVCAR-5). In PEO-1 cells, an increasing trend was observed (*p* value 0.058). GPX4 expression was reduced both at mRNA (RSL3 vs NT: *p* value 0.010 for ES-2; *p* value 0.012 for HEY; *p* value 0.053 for PEO-1; *p* value 0.045 for OVCAR-5) and protein (RSL3 vs NT:

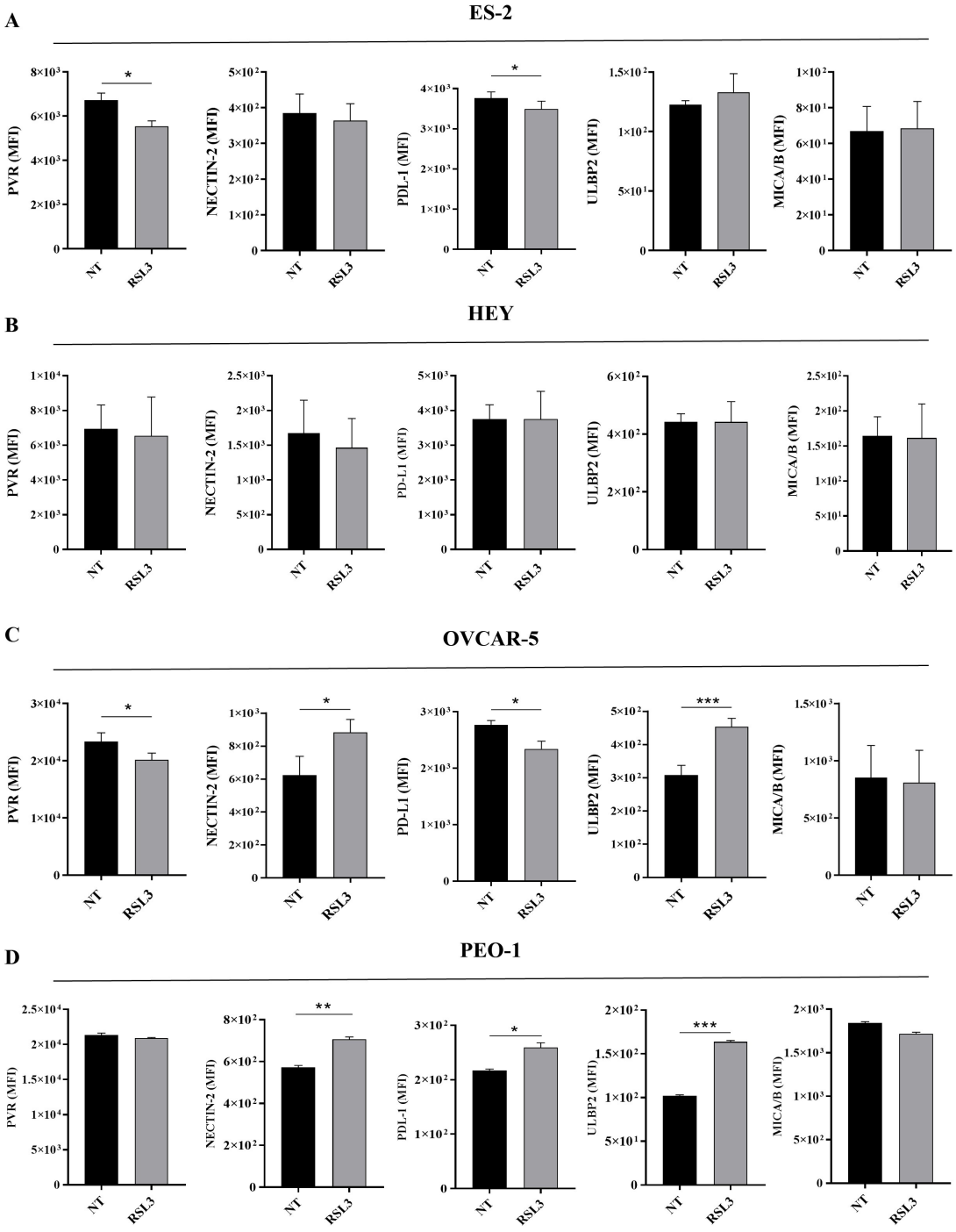

Fig. 5. RSL3 modulates the expression of NK activating and inhibiting molecules on ovarian cancer cell lines. Flow cytometry analysis of PVR, Nectin-2, PD-L1, ULBP2, and MICA/B molecules expressed on (A) ES-2, (B) HEY, (C) OVCAR-5, (D) PEO-1 cells was performed. Statistical analysis is reported. All the experiments were performed in technical and biological triplicates. Data were represented as means ± SD. ***p-value < 0.001; **p-value < 0.01; *p-value < 0.05. A paired two-tailed Student's t test was used. NK, Natural Killer; PVR, Poliovirus Receptor; Nectin-2, Nectin-like molecules-2; MICA/B, MHC class I chain-related protein (MIC) A and B; ULBP2, Unique Long 16-Binding Protein 2; PD-L1, Programmed Death-Ligand 1.

p value 0.00008 for ES-2; p value 0.003 for HEY; p value 0.0001 for PEO-1; p value 0.025 for OVCAR-5) levels in all cell lines.

Co-treatment with Fer-1 and RSL3 modulated RSL3-associated changes at both mRNA and protein levels (Fig. 4 and **Supplementary Fig. 3**). In particular, at mRNA levels, were observed changes in *CD71* (Fer-1 + RSL3 vs RSL3: p

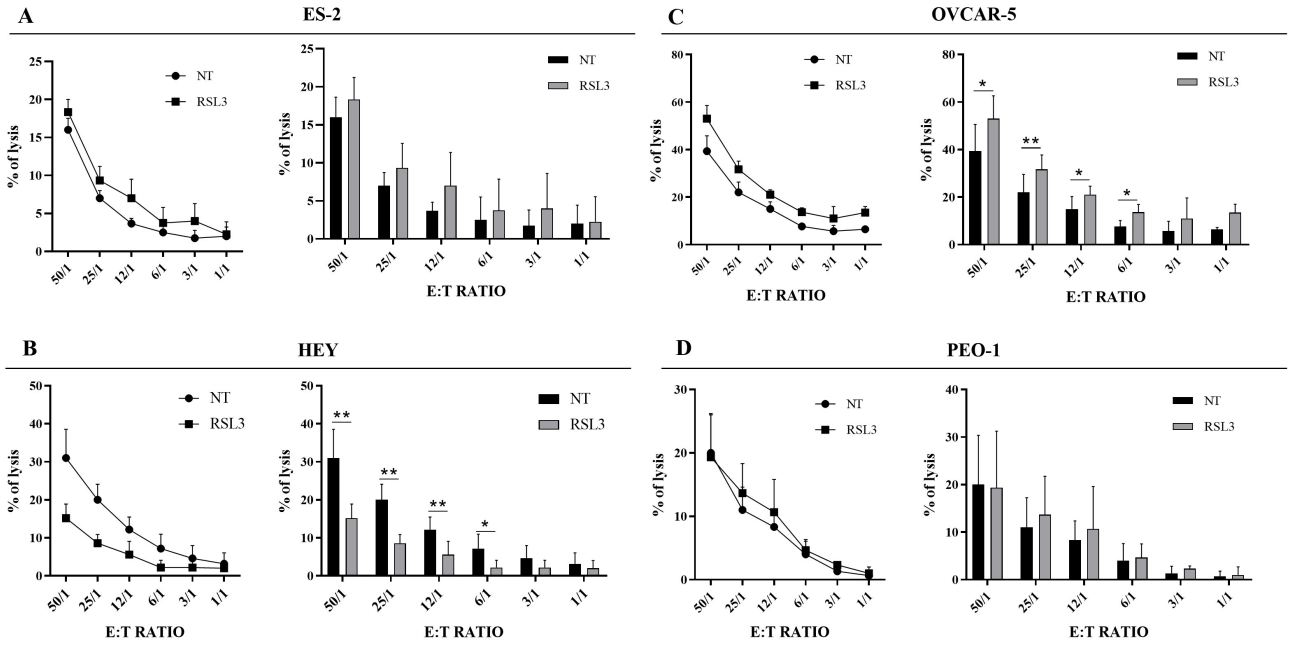

Fig. 6. Susceptibility of RSL3-treated HGOC cell lines to NK cell-mediated killing. Representative experiment (left panel) and statistical analysis (right panel) of cytotoxicity assay against untreated (NT) and RSL3-treated cells are reported. Purified NK cells were used as effector cells. (A) ES-2 were treated with 50 nM of RSL3 for 24 hours. (B) HEY were treated with 1 µM of RSL3 for 24 hours. (C) OVCAR-5 were treated with 5 µM of RSL3 for 24 hours. (D) PEO-1 were treated with 5 µM of RSL3 for 24 hours. Different E:T ratio show the percentage of NK cell lysis of untreated and RSL3-treated cells. All the experiments were performed in technical and biological triplicates. Data were represented as means ± SD. $^{**}p$ value < 0.01; $^{*}p$ value < 0.05. A paired two-tailed Student's t test was used.

value: 0.009 for ES-2; p value 0.029 for OVCAR-5), *NRF2* (Fer-1 + RSL3 vs RSL3: p value 0.011 for HEY; p value 0.008 for PEO-1; p value 0.014 for OVCAR-5), and *GPX4* (Fer-1 + RSL3 vs RSL3: p value 0.002 for ES-2; p value 0.005 for HEY; p value 0.022 for OVCAR-5). No significant changes were observed for *CD71* in HEY and PEO-1 cells, for *NRF2* in ES-2 cells, and for *GPX4* in PEO-1 cells. At the protein levels, changes were observed in CD71 (Fer-1 + RSL3 vs RSL3: p value 0.019 for ES-2), NRF2 (Fer-1 + RSL3 vs RSL3: p value 0.020 for ES-2; p value 0.002 for OVCAR-5), and GPX4 (Fer-1 + RSL3 vs RSL3: p value 0.003 for ES-2; p value 0.011 for PEO-1). No significant changes were observed for CD71 in HEY and OVCAR-5, for NRF2 in HEY and PEO-1 and for GPX4 in HEY and OVCAR-5 cells. All together these results confirm that RSL3 induces ferroptosis in HGOC cell lines. Notably, none of the tested cell lines showed evidence of apoptosis upon exposure to RSL3 (**Supplementary Fig. 4**). Taken together, these results demonstrate that low doses of RSL3 are sufficient to induce ferroptosis in HGOC cell lines, establishing a basis for investigating its role in modulating NK cell-driven anti-tumor immunity.

3.2 NK Cells Recognition of RSL3-treated HGOC Cell Lines

To evaluate whether RSL3-induced ferroptosis directly affects the innate immune response, we performed flow cytometric analysis of surface molecules (PVR, Nectin-2, PD-L1, ULBP2, MICA/B) involved in NK cell recognition (Fig. 5). Treatment with RSL3 led to a reduction of PVR and PD-L1 expression in ES-2 and OVCAR-5 cells (RSL3-treated vs NT: 0.82× fold, p value 0.02 for ES-2; 0.86× fold, p value 0.04 for OVCAR-5 for PVR; 0.92× fold, p value 0.01 for ES-2; 0.84× fold, p value 0.04 for OVCAR-5 for PD-L1; Fig. 5A,C). In contrast, PD-L1 expression was increased in PEO-1 cells, (RSL3-treated vs NT: 1.18× fold, p value 0.013; Fig. 5D), while no significant alterations were observed in HEY cells (Fig. 5B). RSL3 treatment did not significantly alter the expression of Nectin-2 and ULBP2 in ES-2 and HEY cells (Fig. 5A,B), whereas these molecules were significantly upregulated in OVCAR-5 and PEO-1 cells (RSL3-treated vs NT: 1.31× fold, p value 0.01 for OVCAR-5; 1.24× fold, p value 0.002 for PEO-1, for Nectin-2; 1.45× fold, p value 0.0003 for OVCAR-5; 1.6× fold, p value 0.000002 for PEO-1 for ULBP2; Fig. 5C,D). No significant alterations in MICA/B expression were observed across the tested cell lines (Fig. 5A–D). These data indicate that RSL3 modu-

lates the expression of some surface molecules in a cell line-specific manner, reflecting the intrinsic heterogeneity of ovarian cancer.

To determine whether RSL3 treatment influences NK cell-mediated cytotoxicity, we conducted LDH-release assays using purified NK cells from healthy donors co-cultured with HGOC cells at different E:T ratios (Fig. 6). The results demonstrated variable susceptibility among RSL3-treated ovarian cell lines. ES-2 and PEO-1 exhibited minimal lysis (Fig. 6A,D). HEY cells showed a decreased lysis compared to untreated cells (Fig. 6B). Conversely, OVCAR-5 cells displayed a significant increase in NK cell killing following RSL3 treatment (RSL3-treated vs NT: 1.34× fold, p value 0.04 for 50/1; 1.43× fold, p value 0.008 for 25/1; 1.4× fold, p value 0.02 for 12/1; 1.78× fold, p value 0.02 for 6:1 E:T ratios; Fig. 6C). This variability reflects the distinct expression patterns of activating and inhibitory ligands among the different cell lines. In particular, the increased NK cell lysis observed in OVCAR-5 cells appears to be driven by the combined downregulation of inhibitory ligands (PVR, PD-L1) and upregulation of activating ligands (Nectin-2, ULBP2), which facilitates effective immune recognition and cytotoxicity.

Conversely, the absence or insufficient modulation of ligands on ES-2, HEY, and PEO-1 cells results in impaired lysis, leading to either a lack of response or a reduced NK cell-mediated lysis.

In summary, these findings indicate that while RSL3-induced ferroptosis modulates the expression of immune ligands, it alone is insufficient to consistently elicit NK cell-mediated cytotoxicity across all HGOC cell lines.

4. Discussion

The ability of Natural Killer cells to suppress tumors depends on receptor-ligands interaction with molecules displayed on cancer cell membranes [16]. Cancer cells can escape anti-tumor immunity through reduced expression of immune receptors, release of cytokines and soluble immunosuppressive factors, and inhibition of cytotoxic lymphocytes within the TME [14]. The immunosuppressive ovarian TME reduces NK cells' cytotoxic capability and limits the efficacy of immunotherapy, with a percentage of patients developing relapses [8–10,22].

Ferroptosis, a novel identified mechanism of iron-driven cell death, may represent a new and interesting mechanism that makes cancer cells more easily recognizable by the immune system [34–36], as observed in hepatocellular carcinoma [48]. FINs are currently used in preclinical studies to increase the chemosensitivity of HGOC cells [31,32] and may represent potential pharmacological candidates in ovarian cancer therapy [31–33,35]. Based on these observations, we analyzed the effect of RSL3-induced ferroptosis on ovarian cancer cells as a mechanism capable of modulating molecules potentially involved in NK cells–mediated response. First, we identified a minimal dose of RSL3 (Fig. 1) able to induce ferroptosis in HGOC cells through the accumulation of lipid peroxide (Fig. 2) and increased intracellular and mitochondrial ROS formation (Fig. 3). Western blot and qRT-PCR analyses (Fig. 4) shown that in HEY, PEO-1, and OVCAR-5 cells, *Nrf2* mRNA and protein levels follow the pattern already reported in the literature: upon RSL3 treatment, a reduction in *Nrf2* mRNA is observed together with an increase in its protein levels. This increase is not due to enhanced protein synthesis but rather to protein accumulation resulting from impaired KEAP1-mediated degradation [49]. In contrast, ES-2 cells exhibit a decrease in both *Nrf*2 mRNA and protein levels. Reduced NRF2 expression implies a diminished ability to activate major antioxidant and detoxification pathways and to maintain redox homeostasis [50]. Flow cytometry analysis (Fig. 3) further demonstrated that, among all cell lines tested, ES-2 cells display a markedly higher increase in intracellular ROS following treatment compared with their basal levels. This pronounced ROS accumulation is consistent with a compromised antioxidant response caused by the lower NRF2 expression. Collectively, these findings indicate that ES-2 cells are intrinsically more susceptible to RSL3-induced ferroptosis (Fig. 1), suggesting that NRF2 may be regulated differently in this specific ovarian cancer cell line. Data also indicates that Fer-1 also reverts cell viability (**Supplementary Fig. 2A**) and the ferroptotic phenotype as evaluated by reduced lipid peroxides formation and intracellular ROS expression (**Supplementary Fig. 2B**). No evidence of apoptosis was observed in RSL3-treated HGOC cell lines (**Supplementary Fig. 4**).

Here, we hypothesized that RSL3-mediated ferroptosis of HGOC cells modulates NK cell surface molecules, resulting in the possibly NK cell-cytotoxic effect. To assess this hypothesis, we performed an immune-phenotype analysis of RSL3-treated and untreated cells and investigated the main molecules involved in the NK cell-mediated regulation: PVR, Nectin-2, MICA/B, ULBP2 and PD-L1. PVR and Nectin-2 interact with DNAX accessory molecule-1 (DNAM-1), while stress-inducible cell surface proteins MICA/B and ULBP2 bind to NK group 2 member D (NKG2D) receptor, both contribute to the activation of NK cells [20,51,52]. PVR has high affinity also for TIGIT (T cell immunoreceptor with Ig and ITIM domains), essential for NK cell inhibition [53,54]. Also, PD-L1, binding with PD-1 receptor (programmed death-1) exerts a significant NK cell inhibition [55,56].

Our results demonstrated that RSL3 modulates the phenotype of the ovarian cancer cell lines analyzed. Specifically, RSL3 decreased PVR and PD-L1 expression in ES-2 (Fig. 5A) and OVCAR-5 cells (Fig. 5C), suggesting a potential role for RSL3 in limiting the pro-tumoral activity of PVR and PD-L1 in HGOC [27,57–61]. No changes in PVR expression were observed in HEY and PEO-1 cells (Fig. 5B,D). While PD-L1 expression remained unchanged in HEY cells upon RSL3 treatment (Fig. 5B), it was upreg-

ulated in PEO-1 cells (Fig. 5D). Additionally, ULBP2 and Nectin-2 levels were increased in RSL3-treated OVCAR-5 (Fig. 5C) and PEO-1 cells (Fig. 5D). No significant differences in MICA/B expression were detected across any of the cell lines tested (Fig. 5). In line with our data, recent studies indicate that the induction of ferroptosis via iron oxide nanoparticles in prostate cancer upregulates ULBPs, without affecting MICA/B levels thus enhancing NK cell-mediated cytotoxicity [62]. Indeed, despite no direct evidence yet links ferroptosis axes to the regulation of NK-cell ligands, emerging data suggest that IFN- γ released by NK cells induce ferroptosis and kill cancer cells via system Xc-/GSH/GPX4 axis inhibition [63]. Although its role on ligand expression is still unclear, combining ferroptosis induction with NK-based immunotherapy, such as anti-PD-L1, emerges as a promising strategy to overcome tumor immune evasion.

Altogether, our data suggests that ferroptosis may regulate NK-cell ligand expression through molecular mechanisms linked to cellular redox homeostasis. Specifically, the level of NRF2 and the resulting oxidative stress appear to dictate which ligands are modulated, with ROS accumulation promoting the upregulation of stress-inducible activating ligands (such as ULBP2 and Nectin-2) while downregulating inhibitory or pro-tumoral molecules (such as PD-L1 and PVR) in a cell line-specific manner. These findings point to a mechanistic pathway in which ferroptosis-driven oxidative stress serves as a central regulator of NK-ligand expression, providing a molecular basis for the interplay between ferroptosis and NK cell-mediated cytotoxicity.

Based on these observations, we next assessed whether RSL3-driven immune-phenotype alterations in HGOC cells influence their recognition by NK cells.

We demonstrated that ES-2 and PEO-1 are less prone to be killed by NK cells both at baseline and after RSL3 treatment (Fig. 6A,D), while a reduction of lysis in RSL3-treated HEY cells was observed (Fig. 6B). These data indicate that the absence or not balanced signals (activating and inhibitory) from ovarian cancer cells may contribute to defective NK cell lysis. The inadequate interactions between activating and inhibiting NK cell receptors and their cognate ligands contribute to failure of NK cells cytotoxicity [25]. In contrast, RSL3-treated OVCAR-5 cells are more susceptible to NK cell lysis (Fig. 6C), due to the diminished expression of PVR and PD-L1 and increased levels of ULBP2 and Nectin-2 on cell membranes. These findings underscore the ability of NK cells to exert cytotoxic effects on ferroptotic ovarian cancer cells (OVCAR-5) *in vitro*.

However, to fully clarify the therapeutic implications of these findings, *in vivo* validation using patient-derived NK cells is essential, as it would provide valuable insights into the activity of tumor-infiltrating NK cells.

Notably, in three of the four ovarian cancer cell lines analyzed (ES-2, HEY, and PEO-1), despite clear ferroptosis induction evidenced by lipid peroxidation and intracellular ROS accumulation, consistent modulation of ligands sufficient to trigger NK cell recognition was not observed.

Several mechanistic explanations may underlie this differential response. First, compensatory inhibitory pathways may be engaged by tumor cells to counterbalance the pro-immunogenic signals triggered by ferroptotic stress. The persistent or even upregulated expression of inhibitory ligands such as PD-L1, HLA-E, could interact with inhibitory receptors on NK cells (e.g., PD-1, NKG2A), dampening NK cell activation and cytotoxicity. Notably, in PEO-1 cells, PD-L1 was upregulated upon ferroptosis induction, potentially contributing to an immunosuppressive mechanism that blunts NK cell-mediated killing. Furthermore, intrinsic signaling pathways activated in response to ferroptotic stress may promote the secretion of immunosuppressive cytokines or soluble factors that impair NK cell function within the TME. These factors might include TGF-β or IL-10, which are known to inhibit NK cell cytotoxicity and proliferation. All these signals may help explain why some cell lines remain resistant to NK cell killing after ferroptosis induction.

Although our *in vitro* system cannot fully recapitulate the complexity of the TME, previous studies suggest that ferroptosis plays a dual role in shaping tumor immunity. Tumor-associated macrophages (TAMs) and regulatory T cells (Tregs), relatively resistant to ferroptosis due to the high GPX4 expression, may persist and reinforce immunosuppressive conditions, thus impairing NK cell–mediated tumor clearance [64–66]. In contrast, $CD8^+$ T cell-derived IFNγ promotes ferroptotic tumor cell death by altering lipid metabolism and suppressing protective pathways, thereby enhancing responses to immunotherapy [67]. Furthermore, Erastin was shown to induce M2 macrophage polarization via STAT3/IL-8 signaling, thereby promoting the invasiveness of ferroptosis-resistant ovarian cancer cells [68]. Tumor-intrinsic adaptations, such as GPX4 palmitoylation or FABP7-mediated lipid remodeling, can inhibit ferroptosis and reduce immune efficacy, while ferroptosis-resistant Tregs and pro-tumorigenic M2 TAMs may further dampen antitumor immunity [69]. Together, these findings underscore the paradoxical role of ferroptosis as both a mediator of antitumor immunity and, under certain conditions, a promoter of tumor progression [70,71]. Future studies using co-culture models of ovarian TME could provide mechanistic insights into how ferroptosis shapes immune crosstalk and tumor escape.

Taken together, all these considerations emphasize that ferroptosis-induced immunogenicity is not uniform across all tumor cells and is subject to modulation by other mechanisms. Understanding these compensatory inhibitory pathways and tumor-intrinsic factors is crucial to developing combinatorial therapeutic strategies that can overcome immune evasion and harness ferroptosis to potentiate NK cell-mediated anti-tumor immunity.

5. Conclusions

Ovarian cancer heterogeneity and its immunosuppressive microenvironment contribute to therapeutic resistance and poor prognosis. Our findings show that RSL3-induced ferroptosis modulates NK cell ligand expression in HGOC cells but does not uniformly enhance NK cell–mediated tumor clearance. The *in vitro* nature of this work limits the ability to fully recapitulate the complexity of the *in vivo* tumor microenvironment. To address these limitations, future *in vivo* studies will be conducted using NOD/SCID or NSG mice, which permit engraftment of human HGOC cells and infusion of human NK cells. These models will allow assessment of RSL3's therapeutic efficacy, alone or combined with NK cell therapy, by monitoring tumor growth, NK cell infiltration, and ferroptosis-related markers (GPX4 downregulation and lipid peroxidation) within the TME. Moreover, these experiments will help assess how ferroptosis induction influences immune cell dynamics and angiogenesis within the tumor microenvironment.

Collectively, our findings provide the first evidence linking ferroptosis to NK cell recognition in ovarian cancer and highlight the potential of ferroptosis-targeting strategies to enhance immune-based therapies and overcome tumor immune evasion.

Abbreviations

HGOC, High-grade human ovarian cancer; TME, Tumor Microenvironment; EOC, Epithelial Ovarian Cancer; HGSOC, High-Grade Serous Ovarian Cancer; CCOC, Clear Cell Ovarian Cancer; NK, Natural Killer; ILCs, Innate Lymphoid cells; RCD, Regulated Cell Death; ROS, Reactive Oxygen Species; FINs, Ferroptotic Inducers; RSL3, RAS-Selective Lethal 3; PVR, Poliovirus Receptor; Nectin-2, Nectin-like molecules-2; MICA/B, MHC class I chain-related protein (MIC) A and B; ULBP2, Unique Long 16-Binding Protein 2; PD-L1, Programmed Death-Ligand 1; MFI, Median Fluorescence Intensity; DNAM-1, DNAX Accessory Molecule-1; NKG2D, NK group 2 member D; TIGIT, T cell immunoreceptor with Ig and ITIM domains; PD-1, Programmed Death-1; hEOC, human Epithelial Ovarian Cancer; ATCC, American Type Culture Collection; PI, Propidium Iodide; CMH2DCFDA, 2′-7′-Dichlorodihydrofluorescein diacetate; Fer-1, Ferrostatin-1; PBMCs, Peripheral Blood Monocytes Cells; GAPDH, Glyceraldehyde-3-Phosphate Dehydrogenase; GPX4, Glutathione Peroxidase 4; NRF2, NFE2 Like BZIP Transcription Factor 2; LDH, Lactate Dehydrogenase; E:T ratios, Effector : Target Ratio.

Availability of Data and Materials

The datasets used and analyzed during the current study are available from the corresponding author on reasonable request.

Author Contributions

CG and MCF designed the research study. CG, SS, EV performed the research. AN analysed data, provided help and advice on the collection of buffy coat samples derived from healthy donors. CDM provided Mycoplasma detection KIT and STR profiling of all cell lines used, performed the research and analysed data. CG, SS, FB, BQ and BS analyzed the data. CG, SS, MCF, FB, EV, BQ wrote the manuscript. All authors contributed to editorial changes in the manuscript. All authors read and approved the final manuscript. All authors have participated sufficiently in the work and agreed to be accountable for all aspects of the work.

Ethics Approval and Consent to Participate

Informed consent was obtained from all subjects involved in the study. This research follows the Declaration of Helsinki. In accordance with Italian regulations (Legislative Decree 196/2003 as amended by Legislative Decree 101/2018, and EU Regulation 2016/679 – GDPR), this study used residual biological material collected for routine diagnostic purposes. All samples were anonymized prior to analysis. No additional procedures or interventions were performed for research purposes. In line with national regulations, this type of retrospective, anonymized analysis does not require approval from an ethics committee.

Acknowledgment

We thank Caterina Alessi for providing technical support and the "blood transfusion center" of "Pugliese-Ciaccio Hospital", Catanzaro, Italy, for providing buffy-coats.

Funding

This research received no external funding.

Conflict of Interest

The authors declare no conflict of interest. Given her role as the Guest Editor, Flavia Biamonte had no involvement in the peer-review of this article and has no access to information regarding its peer review. Full responsibility for the editorial process for this article was delegated to Sung Eun Kim.

Supplementary Material

Supplementary material associated with this article can be found, in the online version, at https://doi.org/10.31083/FBL46641.

References

[1] Sung H, Ferlay J, Siegel RL, Laversanne M, Soerjomataram I, Jemal A, *et al*. Global Cancer Statistics 2020: GLOBOCAN Estimates of Incidence and Mortality Worldwide for 36 Cancers in

185 Countries. CA: a Cancer Journal for Clinicians. 2021; 71: 209–249. https://doi.org/10.3322/caac.21660.

[2] Lalos A, Neri O, Ercan C, Wilhelm A, Staubli S, Posabella A, *et al*. High Density of CD16+ Tumor-Infiltrating Immune Cells in Recurrent Ovarian Cancer Is Associated with Enhanced Responsiveness to Chemotherapy and Prolonged Overall Survival. Cancers. 2021; 13: 5783. https://doi.org/10.3390/cancers13225783.

[3] Penson RT, Dizon DS, Birrer MJ. Clear cell cancer of the ovary. Current Opinion in Oncology. 2013; 25: 553–557. https://doi.org/10.1097/CCO.0b013e328363e0c7.

[4] Fujiwara K, Shintani D, Nishikawa T. Clear-cell carcinoma of the ovary. Annals of Oncology: Official Journal of the European Society for Medical Oncology. 2016; 27 Suppl 1: i50–i52. https://doi.org/10.1093/annonc/mdw086.

[5] Zhang C, Qin C, Lin Y. Development and Validation of a Prognostic Risk Model Based on Nature Killer Cells for Serous Ovarian Cancer. Journal of Personalized Medicine. 2023; 13: 403. https://doi.org/10.3390/jpm13030403.

[6] Webb JR, Milne K, Watson P, Deleeuw RJ, Nelson BH. Tumor-infiltrating lymphocytes expressing the tissue resident memory marker CD103 are associated with increased survival in high-grade serous ovarian cancer. Clinical Cancer Research: an Official Journal of the American Association for Cancer Research. 2014; 20: 434–444. https://doi.org/10.1158/1078-0432.CCR-13-1877.

[7] Zhang L, Cascio S, Mellors JW, Buckanovich RJ, Osmanbeyoglu HU. Single-cell analysis reveals the stromal dynamics and tumor-specific characteristics in the microenvironment of ovarian cancer. Communications Biology. 2024; 7: 20. https://doi.org/10.1038/s42003-023-05733-x.

[8] Moore KN, Bookman M, Sehouli J, Miller A, Anderson C, Scambia G, *et al*. Atezolizumab, Bevacizumab, and Chemotherapy for Newly Diagnosed Stage III or IV Ovarian Cancer: Placebo-Controlled Randomized Phase III Trial (IMagyn050/GOG 3015/ENGOT-OV39). Journal of Clinical Oncology: Official Journal of the American Society of Clinical Oncology. 2021; 39: 1842–1855. https://doi.org/10.1200/JCO.21.00306.

[9] Pujade-Lauraine E, Fujiwara K, Ledermann JA, Oza AM, Kristeleit R, Ray-Coquard IL, *et al*. Avelumab alone or in combination with chemotherapy versus chemotherapy alone in platinum-resistant or platinum-refractory ovarian cancer (JAVELIN Ovarian 200): an open-label, three-arm, randomised, phase 3 study. The Lancet. Oncology. 2021; 22: 1034–1046. https://doi.org/10.1016/S1470-2045(21)00216-3.

[10] Monk BJ, Colombo N, Oza AM, Fujiwara K, Birrer MJ, Randall L, *et al*. Chemotherapy with or without avelumab followed by avelumab maintenance versus chemotherapy alone in patients with previously untreated epithelial ovarian cancer (JAVELIN Ovarian 100): an open-label, randomised, phase 3 trial. The Lancet. Oncology. 2021; 22: 1275–1289. https://doi.org/10.1016/S1470-2045(21)00342-9.

[11] Blanc-Durand F, Clemence Wei Xian L, Tan DSP. Targeting the immune microenvironment for ovarian cancer therapy. Frontiers in Immunology. 2023; 14: 1328651. https://doi.org/10.3389/fimmu.2023.1328651.

[12] Baci D, Bosi A, Gallazzi M, Rizzi M, Noonan DM, Poggi A, *et al*. The Ovarian Cancer Tumor Immune Microenvironment (TIME) as Target for Therapy: A Focus on Innate Immunity Cells as Therapeutic Effectors. International Journal of Molecular Sciences. 2020; 21: 3125. https://doi.org/10.3390/ijms21093125.

[13] Sun L, Guo YF, Duan CC, Chen C, Xiao L. Post-translational modifications in ovarian cancer: implications for immunotherapy: a mini-review. Journal of Ovarian Research. 2025; 18: 225. https://doi.org/10.1186/s13048-025-01812-1.

[14] Worzfeld T, Pogge von Strandmann E, Huber M, Adhikary T, Wagner U, Reinartz S, *et al*. The Unique Molecular and Cellular Microenvironment of Ovarian Cancer. Frontiers in Oncology. 2017; 7: 24. https://doi.org/10.3389/fonc.2017.00024.

[15] Yan Y, Lu J, Luo H, Wang Z, Xu K, Wang L, *et al*. Decoding immune low-response states in ovarian cancer: insights from single-cell and spatial transcriptomics for precision immunotherapy. Frontiers in Immunology. 2025; 16: 1667464. https://doi.org/10.3389/fimmu.2025.1667464.

[16] Kee BL. Transcriptional control of natural killer cell antitumor activity. Trends in Immunology. 2025; 46: 779–790. https://doi.org/10.1016/j.it.2025.08.007.

[17] Vivier E, Artis D, Colonna M, Diefenbach A, Di Santo JP, Eberl G, *et al*. Innate Lymphoid Cells: 10 Years On. Cell. 2018; 174: 1054–1066. https://doi.org/10.1016/j.cell.2018.07.017.

[18] Zhu W, Fan C, Zhao Y, Li W, Niu J, Dong S, *et al*. The role of NK cells in regulating tumorimmunity: current state, challenges and future strategies. Cancer Cell International. 2025; 25: 360. https://doi.org/10.1186/s12935-025-03980-y.

[19] Farag SS, Caligiuri MA. Human natural killer cell development and biology. Blood Reviews. 2006; 20: 123–137. https://doi.org/10.1016/j.blre.2005.10.001.

[20] Moretta L, Moretta A. Unravelling natural killer cell function: triggering and inhibitory human NK receptors. The EMBO Journal. 2004; 23: 255–259. https://doi.org/10.1038/sj.emboj.7600019.

[21] Ljunggren HG, Kärre K. In search of the 'missing self': MHC molecules and NK cell recognition. Immunology Today. 1990; 11: 237–244. https://doi.org/10.1016/0167-5699(90)90097-s.

[22] Hoogstad-van Evert JS, Bekkers R, Ottevanger N, Jansen JH, Massuger L, Dolstra H. Harnessing natural killer cells for the treatment of ovarian cancer. Gynecologic Oncology. 2020; 157: 810–816. https://doi.org/10.1016/j.ygyno.2020.03.020.

[23] Nersesian S, Arseneau RJ, Mejia JP, Lee SN, Westhaver LP, Griffiths NW, *et al*. Improved overall survival in patients with high-grade serous ovarian cancer is associated with CD16a+ immunologic neighborhoods containing NK cells, T cells and macrophages. Frontiers in Immunology. 2024; 14: 1307873. https://doi.org/10.3389/fimmu.2023.1307873.

[24] Hoogstad-van Evert JS, Maas RJ, van der Meer J, Cany J, van der Steen S, Jansen JH, *et al*. Peritoneal NK cells are responsive to IL-15 and percentages are correlated with outcome in advanced ovarian cancer patients. Oncotarget. 2018; 9: 34810–34820. https://doi.org/10.18632/oncotarget.26199.

[25] Patrizi O, Rampinelli F, Coltrini D, Pesce S, Carlomagno S, Sivori S, *et al*. Natural killer cell impairment in ovarian clear cell carcinoma. Journal of Leukocyte Biology. 2020; 108: 1425–1434. https://doi.org/10.1002/JLB.5MA0720-295R.

[26] Gonzalez-Gugel E, Saxena M, Bhardwaj N. Modulation of innate immunity in the tumor microenvironment. Cancer Immunology, Immunotherapy: CII. 2016; 65: 1261–1268. https://doi.org/10.1007/s00262-016-1859-9.

[27] Carlsten M, Norell H, Bryceson YT, Poschke I, Schedvins K, Ljunggren HG, *et al*. Primary human tumor cells expressing CD155 impair tumor targeting by down-regulating DNAM-1 on NK cells. Journal of Immunology (Baltimore, Md.: 1950). 2009; 183: 4921–4930. https://doi.org/10.4049/jimmunol.0901226.

[28] Petriaggi L, Giorgio E, Natali G, Galeano C, Furtado SR, Faniello CM, *et al*. Iron Fist in a Velvet Glove: Class IV Ferroptosis Inducers as a Novel Strategy to Target Ovarian Cancer. Frontiers in Bioscience (Landmark Edition). 2025; 30: 39675. https://doi.org/10.31083/FBL39675.

[29] Dixon SJ, Olzmann JA. The cell biology of ferroptosis. Nature Reviews. Molecular Cell Biology. 2024; 25: 424–442. https://doi.org/10.1038/s41580-024-00703-5.

[30] Kobayashi H, Yoshimoto C, Matsubara S, Shigetomi H, Imanaka

S. A comprehensive overview of recent developments on the mechanisms and pathways of ferroptosis in cancer: the potential implications for therapeutic strategies in ovarian cancer. Cancer Drug Resistance (Alhambra, Calif.). 2023; 6: 547–566. https://doi.org/10.20517/cdr.2023.49.

[31] Lin CC, Chi JT. Ferroptosis of epithelial ovarian cancer: genetic determinants and therapeutic potential. Oncotarget. 2020; 11: 3562–3570. https://doi.org/10.18632/oncotarget.27749.

[32] Zhou HH, Chen X, Cai LY, Nan XW, Chen JH, Chen XX, *et al*. Erastin Reverses ABCB1-Mediated Docetaxel Resistance in Ovarian Cancer. Frontiers in Oncology. 2019; 9: 1398. https://doi.org/10.3389/fonc.2019.01398.

[33] Cheng Q, Bao L, Li M, Chang K, Yi X. Erastin synergizes with cisplatin via ferroptosis to inhibit ovarian cancer growth in vitro and in vivo. The Journal of Obstetrics and Gynaecology Research. 2021; 47: 2481–2491. https://doi.org/10.1111/jog.14779.

[34] Wang W, Green M, Choi JE, Gijón M, Kennedy PD, Johnson JK, *et al*. CD8$^+$ T cells regulate tumour ferroptosis during cancer immunotherapy. Nature. 2019; 569: 270–274. https://doi.org/10.1038/s41586-019-1170-y.

[35] Battaglia AM, Sacco A, Vecchio E, Scicchitano S, Petriaggi L, Giorgio E, *et al*. Iron affects the sphere-forming ability of ovarian cancer cells in non-adherent culture conditions. Frontiers in Cell and Developmental Biology. 2023; 11: 1272667. https://doi.org/10.3389/fcell.2023.1272667.

[36] Lang X, Green MD, Wang W, Yu J, Choi JE, Jiang L, *et al*. Radiotherapy and Immunotherapy Promote Tumoral Lipid Oxidation and Ferroptosis via Synergistic Repression of SLC7A11. Cancer Discovery. 2019; 9: 1673–1685. https://doi.org/10.1158/2159-8290.CD-19-0338.

[37] Zou Y, Palte MJ, Deik AA, Li H, Eaton JK, Wang W, *et al*. A GPX4-dependent cancer cell state underlies the clear-cell morphology and confers sensitivity to ferroptosis. Nature Communications. 2019; 10: 1617. https://doi.org/10.1038/s41467-019-09277-9.

[38] Battaglia AM, Sacco A, Perrotta ID, Faniello MC, Scalise M, Torella D, *et al*. Iron Administration Overcomes Resistance to Erastin-Mediated Ferroptosis in Ovarian Cancer Cells. Frontiers in Oncology. 2022; 12: 868351. https://doi.org/10.3389/fonc.2022.868351.

[39] Yin J, Chen J, Hong JH, Huang Y, Xiao R, Liu S, *et al*. 4EBP1-mediated SLC7A11 protein synthesis restrains ferroptosis triggered by MEK inhibitors in advanced ovarian cancer. JCI Insight. 2024; 9: e177857. https://doi.org/10.1172/jci.insight.177857.

[40] Scicchitano S, Vecchio E, Battaglia AM, Oliverio M, Nardi M, Procopio A, *et al*. The Double-Edged Sword of Oleuropein in Ovarian Cancer Cells: From Antioxidant Functions to Cytotoxic Effects. International Journal of Molecular Sciences. 2023; 24: 842. https://doi.org/10.3390/ijms24010842.

[41] Scicchitano S, Garofalo C, Stella B, Santamaria G, Cozzolino F, Monaco V, *et al*. Overcoming BET-inhibitor JQ1 resistance in aggressive non-small cell lung cancer by inducing ferroptosis via inhibition of the BRD2-FTH1 axis. The FEBS Journal. 2025. https://doi.org/10.1111/febs.70191. (online ahead of print)

[42] Vecchio E, Marino R, Mimmi S, Canale C, Caiazza C, Arcucci A, *et al*. Enhanced pro-apoptotic activity of rituximab through IBTK silencing in non-Hodgkin lymphoma B-cells. Frontiers in Oncology. 2024; 14: 1339584. https://doi.org/10.3389/fonc.2024.1339584.

[43] Scicchitano S, Gagliardi A, Ambrosio N, Vecchio E, Garofalo C, Battaglia AM, *et al*. Exploring the effects of paclitaxel-loaded zein nanoparticles on human ovarian carcinoma cells. Scientific Reports. 2025; 15: 10553. https://doi.org/10.1038/s41598-025-90840-4.

[44] Di Donato M, Cristiani CM, Capone M, Garofalo C, Madonna G, Passacatini LC, *et al*. Role of the androgen receptor in melanoma aggressiveness. Cell Death & Disease. 2025; 16: 34. https://doi.org/10.1038/s41419-025-07350-4.

[45] Cristiani CM, Capone M, Garofalo C, Madonna G, Mallardo D, Tuffanelli M, *et al*. Altered Frequencies and Functions of Innate Lymphoid Cells in Melanoma Patients Are Modulated by Immune Checkpoints Inhibitors. Frontiers in Immunology. 2022; 13: 811131. https://doi.org/10.3389/fimmu.2022.811131.

[46] Scicchitano S, Montalcini Y, Lucchino V, Melocchi V, Gigantino V, Chiarella E, *et al*. Enhanced ZNF521 expression induces an aggressive phenotype in human ovarian carcinoma cell lines. PloS One. 2022; 17: e0274785. https://doi.org/10.1371/journal.pone.0274785.

[47] Scicchitano S, Faniello MC, Mesuraca M. Zinc Finger 521 Modulates the Nrf2-Notch Signaling Pathway in Human Ovarian Carcinoma. International Journal of Molecular Sciences. 2023; 24: 14755. https://doi.org/10.3390/ijms241914755.

[48] Kong R, Wang N, Han W, Bao W, Lu J. IFNγ-mediated repression of system xc$^-$ drives vulnerability to induced ferroptosis in hepatocellular carcinoma cells. Journal of Leukocyte Biology. 2021; 110: 301–314. https://doi.org/10.1002/JLB.3MA1220-815RRR.

[49] Song Y, Qu Y, Mao C, Zhang R, Jiang D, Sun X. Post-translational modifications of Keap1: the state of the art. Frontiers in Cell and Developmental Biology. 2024; 11: 1332049. https://doi.org/10.3389/fcell.2023.1332049.

[50] Jakubowska M, Costa VM, Krzeptowski W, Dominkuš PP, Santos M, Demirdöğen BC, *et al*. Altered NRF2 signalling in systemic redox imbalance: Insights from non-communicable diseases. Redox Biology. 2025; 87: 103891. https://doi.org/10.1016/j.redox.2025.103891.

[51] Bottino C, Castriconi R, Pende D, Rivera P, Nanni M, Carnemolla B, *et al*. Identification of PVR (CD155) and Nectin-2 (CD112) as cell surface ligands for the human DNAM-1 (CD226) activating molecule. The Journal of Experimental Medicine. 2003; 198: 557–567. https://doi.org/10.1084/jem.20030788.

[52] Lanier LL. NK cell recognition. Annual Review of Immunology. 2005; 23: 225–274. https://doi.org/10.1146/annurev.immunol.23.021704.115526.

[53] Kruse PH, Matta J, Ugolini S, Vivier E. Natural cytotoxicity receptors and their ligands. Immunology and Cell Biology. 2014; 92: 221–229. https://doi.org/10.1038/icb.2013.98.

[54] Yu X, Harden K, Gonzalez LC, Francesco M, Chiang E, Irving B, *et al*. The surface protein TIGIT suppresses T cell activation by promoting the generation of mature immunoregulatory dendritic cells. Nature Immunology. 2009; 10: 48–57. https://doi.org/10.1038/ni.1674.

[55] Chan CJ, Martinet L, Gilfillan S, Souza-Fonseca-Guimaraes F, Chow MT, Town L, *et al*. The receptors CD96 and CD226 oppose each other in the regulation of natural killer cell functions. Nature Immunology. 2014; 15: 431–438. https://doi.org/10.1038/ni.2850.

[56] Pesce S, Greppi M, Tabellini G, Rampinelli F, Parolini S, Olive D, *et al*. Identification of a subset of human natural killer cells expressing high levels of programmed death 1: A phenotypic and functional characterization. The Journal of Allergy and Clinical Immunology. 2017; 139: 335–346.e3. https://doi.org/10.1016/j.jaci.2016.04.025.

[57] Pesce S, Greppi M, Grossi F, Del Zotto G, Moretta L, Sivori S, *et al*. PD/1-PD-Ls Checkpoint: Insight on the Potential Role of NK Cells. Frontiers in Immunology. 2019; 10: 1242. https://doi.org/10.3389/fimmu.2019.01242.

[58] Smazynski J, Hamilton PT, Thornton S, Milne K, Wouters MCA, Webb JR, *et al*. The immune suppressive factors CD155 and PD-

L1 show contrasting expression patterns and immune correlates in ovarian and other cancers. Gynecologic Oncology. 2020; 158: 167–177. https://doi.org/10.1016/j.ygyno.2020.04.689.

[59] Huang LJ, Deng XF, Chang F, Wu XL, Wu Y, Diao QZ. Prognostic significance of programmed cell death ligand 1 expression in patients with ovarian carcinoma: A systematic review and meta-analysis. Medicine. 2018; 97: e12858. https://doi.org/10.1097/MD.0000000000012858.

[60] Zhu J, Wen H, Bi R, Wu Y, Wu X. Prognostic value of programmed death-ligand 1 (PD-L1) expression in ovarian clear cell carcinoma. Journal of Gynecologic Oncology. 2017; 28: e77. https://doi.org/10.3802/jgo.2017.28.e77.

[61] Parvathareddy SK, Siraj AK, Al-Badawi IA, Tulbah A, Al-Dayel F, Al-Kuraya KS. Differential expression of PD-L1 between primary and metastatic epithelial ovarian cancer and its clinicopathological correlation. Scientific Reports. 2021; 11: 3750. https://doi.org/10.1038/s41598-021-83276-z.

[62] Kim KS, Choi B, Choi H, Ko MJ, Kim DH, Kim DH. Enhanced natural killer cell anti-tumor activity with nanoparticles mediated ferroptosis and potential therapeutic application in prostate cancer. Journal of Nanobiotechnology. 2022; 20: 428. https://doi.org/10.1186/s12951-022-01635-y.

[63] Tang D, Kroemer G, Kang R. Ferroptosis in immunostimulation and immunosuppression. Immunological Reviews. 2024; 321: 199–210. https://doi.org/10.1111/imr.13235.

[64] Xu H, Lu Y, Zeng Q, Zhu X, Guan W, Liu S. Ferroptosis of Immune Cells in Infection, Inflammation and Tumor Progression. Biomolecules. 2025; 15: 1464. https://doi.org/10.3390/biom15101464.

[65] Wu X, Liu Q, Jiang Z, Wang G, Liao L, Ye X, *et al*. Targeting ferroptosis: a promising avenue for ovarian cancer treatment. Frontiers in Immunology. 2025; 16: 1578723. https://doi.org/10.3389/fimmu.2025.1578723.

[66] Xu C, Sun S, Johnson T, Qi R, Zhang S, Zhang J, *et al*. The glutathione peroxidase Gpx4 prevents lipid peroxidation and ferroptosis to sustain Treg cell activation and suppression of antitumor immunity. Cell Reports. 2021; 35: 109235. https://doi.org/10.1016/j.celrep.2021.109235.

[67] Liao P, Wang W, Wang W, Kryczek I, Li X, Bian Y, *et al*. $CD8^+$ T cells and fatty acids orchestrate tumor ferroptosis and immunity via ACSL4. Cancer Cell. 2022; 40: 365–378.e6. https://doi.org/10.1016/j.ccell.2022.02.003.

[68] Cang W, Wu A, Gu L, Wang W, Tian Q, Zheng Z, *et al*. Erastin enhances metastatic potential of ferroptosis-resistant ovarian cancer cells by M2 polarization through STAT3/IL-8 axis. International Immunopharmacology. 2022; 113: 109422. https://doi.org/10.1016/j.intimp.2022.109422.

[69] Cui K, Wang K, Huang Z. Ferroptosis and the tumor microenvironment. Journal of Experimental & Clinical Cancer Research: CR. 2024; 43: 315. https://doi.org/10.1186/s13046-024-03235-0.

[70] Zhou L, Lian G, Zhou T, Cai Z, Yang S, Li W, *et al*. Palmitoylation of GPX4 via the targetable ZDHHC8 determines ferroptosis sensitivity and antitumor immunity. Nature Cancer. 2025; 6: 768–785. https://doi.org/10.1038/s43018-025-00937-y.

[71] Freitas-Cortez MA, Masrorpour F, Jiang H, Mahmud I, Lu Y, Huang A, *et al*. Cancer cells avoid ferroptosis induced by immune cells via fatty acid binding proteins. Molecular Cancer. 2025; 24: 40. https://doi.org/10.1186/s12943-024-02198-2.